Amino Acids (2014) 46:1547–1556
DOI 10.1007/s00726-014-1727-x

ORIGINAL ARTICLE

Near-infrared fluorescence imaging of CD13 receptor expression using a novel Cy5.5-labeled dimeric NGR peptide

Guoquan Li · Yan Xing · Jing Wang · Peter S. Conti · Kai Chen

Received: 7 March 2014 / Accepted: 7 March 2014 / Published online: 21 March 2014

Abstract In this study, we synthesized a novel Cy5.5-labeled dimeric NGR peptide (Cy5.5-NGR2) via bioorthogonal click chemistry, and evaluated the utility of Cy5.5-NGR2 for near-infrared fluorescence imaging of CD13 receptor expression in vivo. The dimeric NGR peptide (NGR2) was conjugated with an alkyne-containing PEG unit followed by mixing with an azide-terminated Cy5.5 fluorophore (Cy5.5-N_3) to afford Cy5.5-NGR2. The probe was subject to in vitro and in vivo evaluations. The bioorthogonal click chemistry provided a rapid conjugation of the alkyne-containing NGR2 with Cy5.5-N_3 in a quantitative yield within 15 min. The laser confocal microscopy revealed that binding of Cy5.5-NGR2 to CD13 receptor is target-specific as demonstrated in CD13-positive HT-1080 cells, CD13-negative MCF-7 cells, and a blocking study in HT-1080 cells. For in vivo optical imaging, Cy5.5-NGR2 exhibited rapid HT-1080 tumor targeting at 0.5 h postinjection (pi), and highest tumor-to-background contrast at 2 h pi. The CD13-specific tumor accumulation of Cy5.5-NGR2 was accomplished by a blocking study with unlabeled NGR peptide in HT-1080 tumor bearing mice. The tumor-to-muscle ratio of Cy5.5-NGR2 at 2 h pi reached 2.65 ± 0.13 in the non-blocking group vs. 1.05 ± 0.06 in the blocking group. The results from ex vivo imaging were consistent with the in vivo findings. We concluded that Cy5.5-NGR2 constructed by bioorthogonal click chemistry is a promising molecular probe, not only allowing the NIR optical imaging of CD13 overexpressed tumors, but also having the potential to facilitate noninvasive monitoring of CD13-targeted tumor therapy.

Keywords Molecular imaging probe · NGR peptide · Fluorescence imaging · CD13 receptor · Tumor vasculature

Abbreviations

NIRF	Near-infrared fluorescence
PET	Positron emission tomography
SPECT	Single photon emission computed tomography
CT	Computed tomography
MRI	Magnetic resonance imaging
APN	Aminopeptidase N
NGR	Asparagine–glycine–arginine
HPLC	High-performance liquid chromatography
PBS	Phosphate-buffered saline
DBCO	Dibenzocyclooctyne
NHS	*N*-Hydroxysuccinimide
TFA	Trifluoroacetic acid
DMSO	Dimethyl sulfoxide
DAPI	4′,6-Diamidino-2-phenylindole
PFA	Paraformaldehyde
Pi	Postinjection
ROI	Region-of-interest
^{18}F-FDG	^{18}F-Fluorodeoxyglucose
PK	Pharmacokinetics

Introduction

Near-infrared fluorescence (NIRF) optical imaging is an excellent noninvasive technique for studying diseases at

G. Li · J. Wang (✉)
Department of Nuclear Medicine, Xijing Hospital, The Fourth Military Medical University, Xi'an 710032, Shaanxi, China
e-mail: wangjing@fmmu.edu.cn

G. Li · Y. Xing · P. S. Conti · K. Chen (✉)
Molecular Imaging Center, Department of Radiology, Keck School of Medicine, University of Southern California, 2250 Alcazar Street, CSC 103, Los Angeles, CA 90033-9061, USA
e-mail: chenkai@usc.edu

the molecular level in living subjects (Weissleder et al. 1999; Tung 2004; Chen et al. 2004; Kobayashi et al. 2010). As compared to nuclear imaging techniques, such as positron emission tomography (PET) and single photon emission computed tomography (SPECT), NIRF imaging does not employ ionizing radiation or radioactive materials, rendering it cost-effective, robust, sensitive, and straightforward over other imaging modalities (Chen et al. 2004, 2012b). Although absorption and scattering from biological tissues may limit penetration of light through the body, photon penetration into and out of tissue can be more efficient in the near-infrared window (650–900 nm) with minimal intra-tissue scattering. Recent research advances have demonstrated that optical imaging is playing a valuable role in better understanding of biology, early diagnosis of diseases, and effective assessment of treatment (Sakatani et al. 1997; Wunderbaldinger et al. 2003; Raymond et al. 2008; Kobayashi et al. 2010).

Tumor angiogenesis is a complex, multi-step process, in which five phases can be distinguished, including (1) endothelial cell activation, (2) basement membrane degradation, (3) endothelial cell migration, (4) vessel formation, and (5) angiogenic remodeling (Carmeliet 2000). All these tumor angiogenesis events are specifically mediated and controlled by a number of biomarkers (Chen and Chen 2011b; Ellis et al. 2001; Kuwano et al. 2001; Yancopoulos et al. 2000). Consequently, biomarkers exclusively expressed in tumor angiogenesis were recognized to be potential targets for cancer diagnosis and therapy. Numerous studies have proved that CD13 receptor is an important regulator of endothelial morphogenesis during tumor angiogenesis (Bhagwat et al. 2001). CD13 receptor, also known as aminopeptidase N (APN), is a zinc-dependent membrane-bound ectopeptidase that degrades preferentially proteins and peptides with an *N*-terminal neutral amino acid (Guzman-Rojas et al. 2012). The full length of CD13 consists of 967 amino acids with a short N-terminal cytoplasmic domain, a single transmembrane part, and a large cellular ectodomain containing the active site (Luan and Xu 2007). A sizable body of evidence suggests that overexpression of CD13 is associated with the progression of many tumors, such as prostate, colon, and pancreatic cancer (Teranishi et al. 2008; Ikeda et al. 2003; Hashida et al. 2002). Through in vivo screening of a phage-displayed peptide library, a tumor vasculature-homing phage carrying sequence CNGRCVSGCAGRC was selected by using human breast carcinoma xenografts (Arap et al. 1998). Later, the molecular basis behind NGR tumor-homing properties was revealed, and NGR-containing peptide was identified as a specific ligand for CD13 receptor (Pasqualini et al. 2000). Since then, a number of NGR-containing derivatives have been developed for both CD13-targeted tumor imaging and therapy (von Wallbrunn et al. 2008; Negussie et al. 2010; Wang et al. 2011).

Recently, we made use of the bivalency principle to develop a novel dimeric NGR peptide (NGR2), which exhibits subnanomolar affinity to CD13 overexpressed tumor cells (Chen et al. 2013). We also radiolabeled the NGR2 peptide with ^{64}Cu, and the resulting PET probe displayed favorable in vivo performance in terms of high tumor uptake and slow tumor washout in CD13-positive tumor xenografts. We thus hypothesized that the newly developed NGR2 peptide could be an excellent candidate for developing an optical imaging probe, which may allow the NIR optical imaging of CD13 overexpressed tumors and facilitate noninvasive monitoring of CD13-targeted tumor therapy in the near future. In this report, an alkyne-containing NGR2 peptide was synthesized and conjugated rapidly and quantitatively with Cy5.5-N_3 through bioorthogonal click chemistry. The resulting Cy5.5-NGR2 peptide was further evaluated by in vitro and in vivo studies to explore its functions and utility as a CD13-specific NIRF imaging probe.

Materials and methods

General

All chemicals (reagent grade) were obtained from commercial suppliers and used without further purification. The monomeric NGR peptide [GGGCNGRC; disulfide Cys:-Cys = 4–8] was purchased from C S Bio, Inc. (Menlo Park, CA, USA). The Cy5.5 azide (Cy5.5-N_3) was purchased from Lumiprobe Corporation (Hallandale Beach, FL, USA). The DBCO-PEG_4-NHS ester was purchased from Click Chemistry Tools, Inc. (Scottsdale, AZ, USA). Mass spectra were obtained on a Q-Tof premier-UPLC system equipped with an electrospray interface (ESI) (Waters Corporation, Milford, MA, USA).

HPLC methods

Analytical reversed phase HPLC was accomplished on two Waters 515 HPLC pumps, a Waters 2487 absorbance UV detector, which were operated by Waters Empower 2 software. The UV absorbance was monitored at 214 and 254 nm. The purification of DBCO-conjugated NGR2 peptide was performed on a Phenomenex Luna C18 reversed phase column (5 µm, 250 × 4.6 mm). The flow rate was 1 mL/min with the mobile phase starting from 100 % solvent A (0.1 % TFA in water) to 40 % solvent A and 60 % solvent B (0.1 % TFA in acetonitrile) at 22.5 min. The purification of Cy5.5-NGR2 peptide was performed on the same HPLC column. The flow rate was 1 mL/min with the mobile phase starting from 100 % solvent A (0.1 %

TFA in water) to 5 % solvent A and 95 % solvent B (0.1 % TFA in acetonitrile) at 30 min.

Synthesis of DBCO-conjugated NGR2 peptide

The dimeric NGR peptide (NGR2) was prepared according to a procedure described previously (Chen et al. 2013). To a solution of the NGR2 peptide (4.0 mg, 2.6 μmol) in 200 μL of sodium borate buffer (pH = 8.5) was added DBCO-PEG_4-NHS ester (2.0 mg, 3.1 μmol) dissolved in 20 μL of DMSO. The mixture was adjusted to pH 8.5 and sonicated at room temperature for 1 h. The crude peptide was purified by HPLC. The peak containing the desired product was collected and lyophilized to afford a fluffy white powder (4.1 mg, yield: 76 %).

Synthesis of Cy5.5-NGR2 peptide

To a solution of the DBCO-conjugated NGR2 peptide (1.0 mg, 0.48 μmol) in 100 μL of phosphate buffered saline (PBS) was added Cy5.5 azide (0.35 mg, 0.53 μmol) dissolved in 10 μL of DMSO and 100 μL of acetonitrile. The mixture was shaken in the dark at room temperature for 15 min. The crude peptide was purified by HPLC. The peak containing the desired product was collected, lyophilized, and stored in the dark at −20 °C until use (1.2 mg, yield 91 %).

Absorption and emission spectra

The absorption spectrum of Cy5.5-NGR2 peptide was recorded on a Cary 14 UV–Vis spectrometer (Bogart, GA, USA). The spectrum was scanned from 550 to 800 nm with an increment of 1 nm. The fluorescence emission of Cy5.5-NGR2 peptide was measured using a Shimadzu RF-5301PC spectrofluorophotometer (Columbia, MD, USA), and the spectrum was scanned from 550 to 800 nm with an increment of 1 nm. The wavelength of excitation light was set at 650 nm.

Cell line and culture condition

HT-1080 human fibrosarcoma cell line and MCF-7 human breast cancer cell line were obtained from the American Type Culture Collection (ATCC, Manassas, VA, USA). HT-1080 and MCF-7 cells were grown in Dulbecco's modified Eagle's medium(DMEM) (USC Cell Culture Core, Los Angeles, CA, USA) supplemented with 10 % fetal bovine serum (FBS) at 37 °C in humidified atmosphere containing 5 % CO_2.

In vitro fluorescence imaging of Cy5.5-NGR2

HT-1080 and MCF-7 cells were grown in chamber slides (VWR Corporate, Radnor, PA, USA) with a density of 2×10^4/well for 24 h. After washing with serum-free DMEM medium for 3 min, the cells in each well were fixed with 2 % paraformaldehyde (PFA) for 10 min, and then washed with serum-free DMEM medium (3 times, 3 min/wash). The HT-1080 or MCF-7 cells were incubated with 20 nM of Cy5.5-NGR2 peptide in 200 μL of serum-free DMEM medium at 37 °C in the dark for 15 min, followed by the PBS wash (3 times, 5 min/wash). For the blocking group, the HT-1080 cells were co-incubated with 20 nM of Cy5.5-NGR2 peptide and 50 μM of unlabeled monomeric NGR peptide. The chamber slide was then mounted with a DAPI (4′,6-diamidino-2-phenylindole) containing mounting medium, and placed under a Zeiss LSM 510 confocal laser scanning microscope (Carl Zeiss Microscopy, LLC, Thornwood, NY, USA).

Animal model

All animal procedures were performed according to a protocol approved by University of Southern California Institutional Animal Care and Use Committee. Female athymic nude mice (about 4–6 weeks old, with a body weight of 20–25 g) were obtained from Harlan Laboratories (Livermore, CA, USA). The HT-1080 tumor xenografts were generated by subcutaneous injection of 5×10^6 HT-1080 cells suspended in 50 μL of cell culture media and 50 μL of BD Matrigel (BD Biosciences, San Jose, CA, USA) into the right shoulder of mice. The cells were allowed to grow 2 weeks until tumors were 200–300 mm^3 in volume. Tumor growth was measured using caliper measurements in orthogonal dimensions.

In vivo and ex vivo near-infrared fluorescence imaging

In vivo fluorescence imaging was performed using the IVIS Imaging System 200 Series and analyzed using the IVIS Living Imaging 4.4 software (PerkinElmer Inc., Alameda, CA, USA). A Cy5.5 filter set was used for acquiring the fluorescence of Cy5.5-NGR2 peptide. Identical illumination settings (lamp voltage, filters, f/stop, field of views, binning) were used for acquiring all images. Fluorescence emission images were normalized and reported as photons per second per centimeter squared per steradian (p/s/cm^2/sr). The mice in the non-blocking group ($n = 3$) received 1.5 nmol of Cy5.5-NGR2 intravenously and subjected to optical imaging at various time points postinjection (pi). The mice in the blocking group ($n = 3$) were injected with a mixture of Cy5.5-NGR2 peptide (1.5 nmol) and unlabeled monomeric NGR peptide (20 mg/kg). All near-infrared fluorescence images were acquired using 1 s exposure time (f/stop = 4). Mice from the non-blocking and blocking groups were euthanized at 4 h pi. The tumors, tissues, and organs were dissected and subjected to ex vivo

fluorescence imaging. The mean fluorescence for each sample was reported.

Data processing and statistical analysis

All of the data were presented as mean ± SD (standard deviation) of n independent measurements. Statistical analysis was performed with a Student's t test. Statistical significance was assigned for P values <0.05. To determine tumor contrast, mean fluorescence intensities of the tumor (T) area at the right shoulder of the animal and of the normal tissue (N) at the surrounding tissue were calculated using the region-of-interest (ROI) function of the IVIS Living Image 4.4 software. Dividing T by N yielded the contrast between tumor and normal tissue.

Results

Syntheses and characterizations of DBCO-conjugated NGR2 peptide and Cy5.5-NGR2

The schematic molecular structure of Cy5.5-NGR2 peptide was shown in Fig. 1. Preparation of Cy5.5-NGR2 peptide was achieved in two steps starting from the dimeric NGR peptide (NGR2) with an overall yield of 69 %. In the first step, the PEGylated-DBCO NHS ester was coupled onto the amino group of the NGR2 peptide. The azide-containing Cy5.5 fluorophore (Cy5.5-N_3) was then reacted with DBCO-conjugated NGR2 peptide in PBS. The catalyst-free click chemistry provided a rapid conjugation of the alkyne-containing NGR2 with Cy5.5-N_3 in a quantitative yield within 15 min. The desired Cy5.5-NGR2 was isolated through HPLC purification and the purity was over 98 %. The retention time of DBCO-conjugated NGR2 peptide and Cy5.5-NGR2 on analytical HPLC was 16.3 min and 23.8 min, respectively. ESI mass spectrometry yielded m/z = 1,044.50 ($[M+2H]^{2+}$) for DBCO-conjugated NGR2 peptide (calculated $[M+2H]^{2+}$ = 1,044.63 for $C_{83}H_{119}N_{27}O_{29}S_4$) and m/z = 932.07 ($[M+2Na]^{3+}$) for Cy5.5-NGR2 (calculated $[M+2Na]^{3+}$= 932.38 for $C_{126}H_{168}N_{33}O_{30}S_4$).

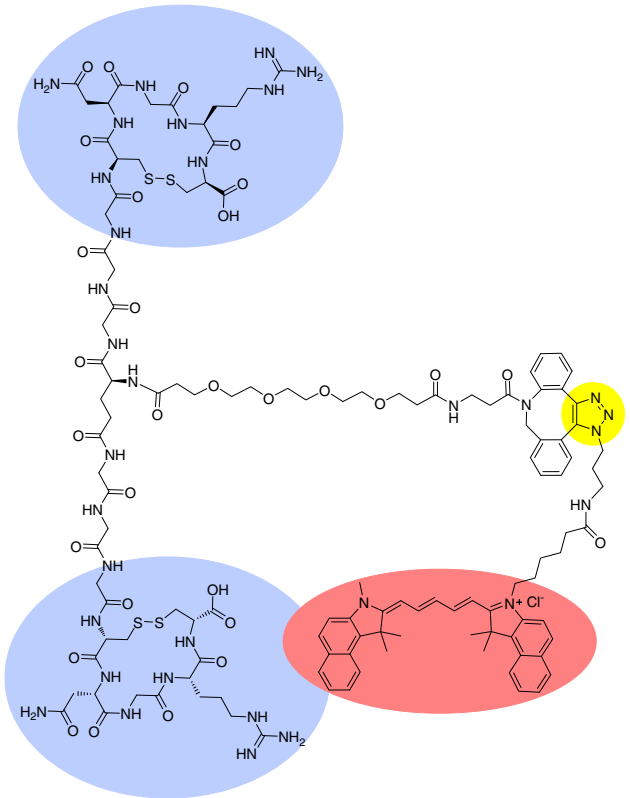

Fig. 1 Schematic structure of the Cy5.5-NGR2 peptide

Absorption and emission spectra

The absorption and fluorescence emission spectra of the Cy5.5-NGR2peptide were shown in Fig. 2. The maximum absorption and fluorescence emission wavelength of Cy5.5-NGR2 was determined to be 674 and 703 nm, respectively.

Binding specificity of Cy5.5-NGR2

To determine the CD13 binding specificity and subcellular localization of Cy5.5-NGR2, the probe was incubated with CD13-positive HT-1080 tumor cells and laser confocal microscopic imaging was carried out after 15 min incubation at 37 °C. Intensive fluorescent signal was observed from the membrane of HT-1080 cells, and some fluorescent signals were also found to be in the cytoplasm of the cells

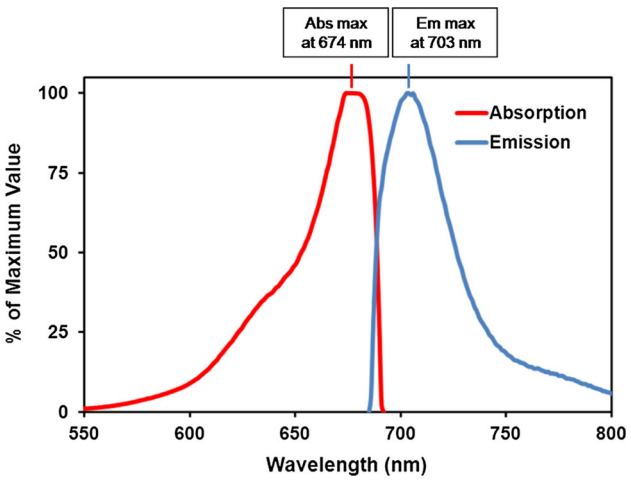

Fig. 2 Absorption and emission fluorescence spectra of Cy5.5-NGR2 peptide

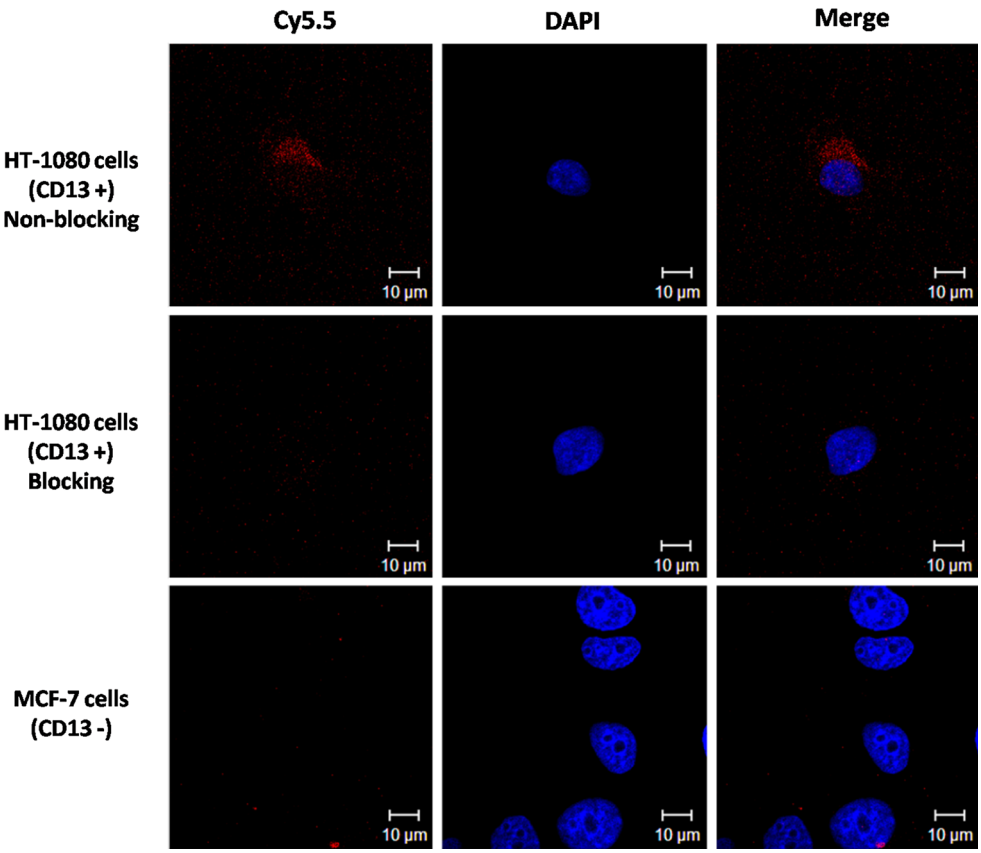

Fig. 3 Confocal microscopy results of Cy5.5-NGR2 with HT-1080 cells (CD13 positive) and MCF-7 cells (CD13 negative) (magnification ×100). The blocking study can be achieved by adding unlabeled monomeric NGR peptide. Top: incubation of Cy5.5-NGR2 (20 nM) with CD13-positive HT-1080 cells; Middle: incubation of Cy5.5-NGR2 (20 nM) with CD13-positive HT-1080 cells blocked by an unlabeled monomeric NGR peptide (50 μM); Bottom: incubation of Cy5.5-NGR2 (20 nM) with CD13-negative MCF-7 cells

(Fig. 3, top). In addition, the fluorescent signal from the cells could be significantly reduced by incubation of the HT-1080 cells with large excess of the unlabeled monomeric NGR peptide (50 μM) (Fig. 3, middle). Furthermore, the staining of Cy5.5-NGR2 in low CD13-expressed MCF-7 cells was barely visible (Fig. 3, bottom). Taken together, the laser confocal microscopy results demonstrated that Cy5.5-NGR2 binds to CD13 receptor specifically.

In vivo and ex vivo near-infrared fluorescence imaging

NIR fluorescence images of nude mice bearing subcutaneous HT-1080 tumor were acquired after intravenous injection of 1.5 nmol of Cy5.5-NGR2 (Fig. 4a). Cy5.5-NGR2 exhibited a rapid HT-1080 tumor targeting as early as at 0.5 h pi. Good contrast to background tissue of Cy5.5-NGR2 in HT-1080 tumors can be visualized from 1 to 3 h pi, and highest tumor-to-background contrast was observed at 2 h pi. Fluorescence intensities in HT-1080 tumor and muscle were plotted as a function of time (Fig. 4b). The HT-1080 tumor uptake reached a maximum at 2 h pi and slowly washed out over time. In contrast, the normal tissue had faster probe binding and washout. The overall uptake of Cy5.5-NGR2 in muscle was significantly lower as compared to tumor during 4-h study period.

The CD13 specificity of Cy5.5-NGR2 was verified by a blocking experiment. For the blocking group, each HT-1080 tumor bearing mouse was intravenously co-injected with 1.5 nmol of Cy5.5-NGR2 and unlabeled monomeric NGR peptide (20 mg/kg), whereas mice in the non-blocking group were injected with 1.5 nmol of Cy5.5-NGR2 only. The results showed that the unlabeled monomeric NGR peptide significantly reduced HT-1080 tumor uptake and tumor contrast at all imaging time points. The optical images of HT-1080 tumor bearing mice at 2 h pi from the non-blocking and blocking group were presented in Fig. 5a. Tumor contrast as quantified by the ROI analysis of images indicated that the tumor-to-muscle value at 2 h pi was reduced from 2.65 ± 0.13 to 1.05 ± 0.06 ($P < 0.05$) (Fig. 5b).

Furthermore, the results from ex vivo imaging were consistent with the in vivo findings. Ex vivo evaluation of excised organs at 4 h pi of Cy5.5-NGR2 showed predominant probe uptake in the non-blocking HT-1080 tumors, whereas significant reduction of HT-1080 uptake was observed in the blocking group (Fig. 6a). Aside from the HT-1080 tumor, liver uptake of Cy5.5-NGR2 remained higher than the amounts measured in other major organs. Quantitative data analysis using ROI of the organs was plotted in Fig. 6b. In the non-blocking group, Cy5.5-NGR2

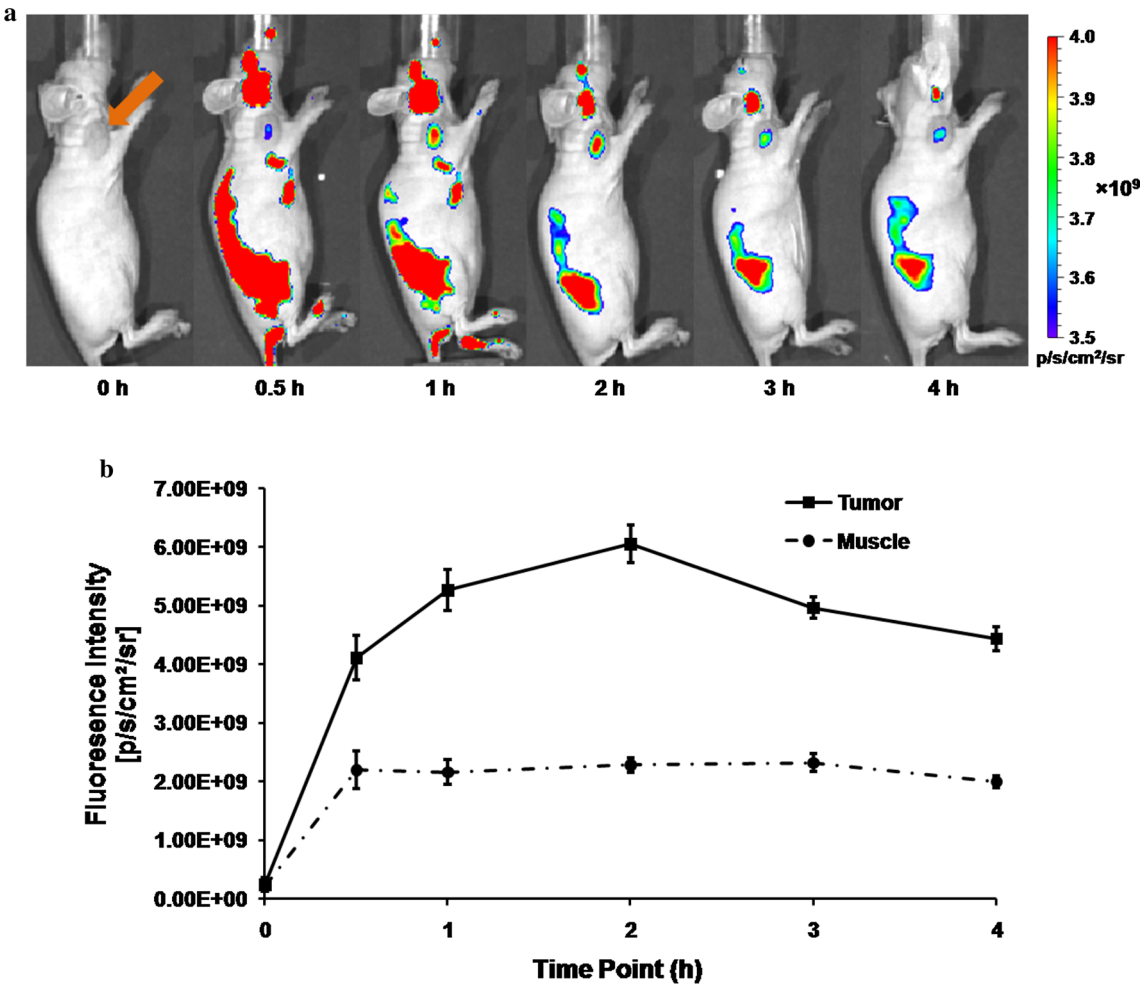

Fig. 4 **a** Time-course fluorescence imaging of subcutaneous HT-1080 tumor bearing nude mice after intravenous injection of 1.5 nmol of Cy5.5-NGR2. The tumors can be clearly visualized as indicated by an *arrow* from 0.5 to 4 h pi. The fluorescence intensity was recorded as per second per centimeter squared per steradian (p/s/cm^2/sr). **b** Quantification and kinetics of in vivo targeting character of Cy5.5-NGR2 in the HT-1080 tumor vs. muscle. The Cy5.5-NGR2 uptake in HT-1080 tumor at various time points was significantly higher than that in muscle. *Error bar* was calculated as the standard deviation ($n = 3$)

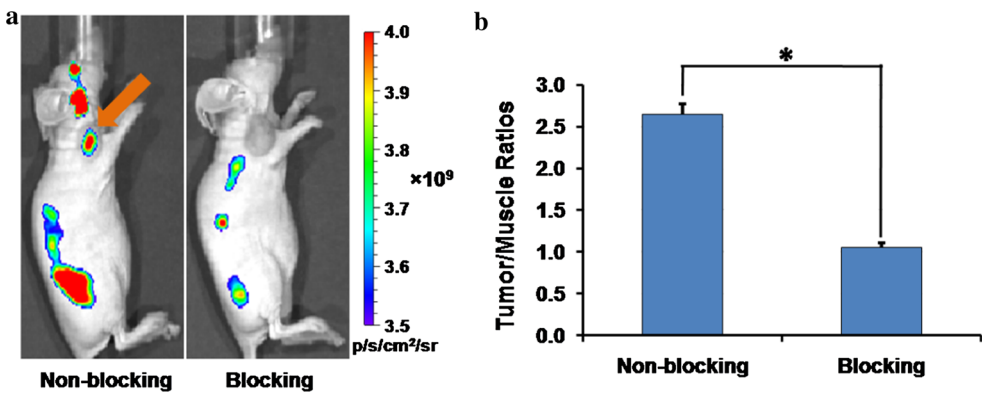

Fig. 5 **a** Representative optical imaging (at 2 h pi) of mice bearing HT-1080 tumor on the right shoulder demonstrating blocking of Cy5.5-NGR2 (1.5 nmol) uptake by co-injection with unlabeled monomeric NGR peptide (20 mg/kg). **b** Fluorescence intensity ratio of tumor-to-muscle based on the ROI analysis of Cy5.5-NGR2 uptake at 2 h pi in HT-1080 tumors without (non-blocking) or with (blocking) co-injection of unlabeled monomeric NGR peptide (20 mg/kg). *Error bar* was calculated as the standard deviation ($n = 3$)

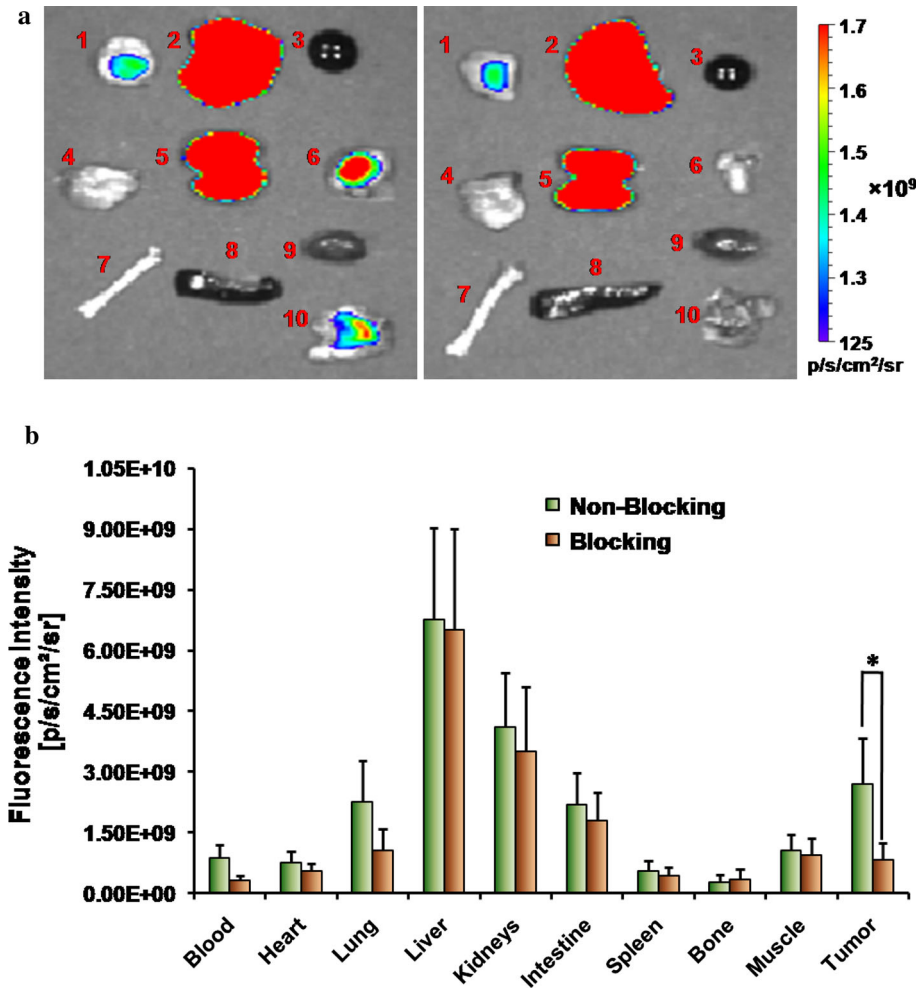

Fig. 6 **a** Ex vivo imaging of tumor and normal tissues with Cy5.5-NGR2 (1.5 nmol) after euthanizing the mice at 4 h pi; *1* Intestine, *2* liver, *3* blood, *4* muscle, *5* kidneys, *6* tumor, *7* bone, *8* spleen, *9* heart, and *10* lung. **b** ROI analysis of ex vivo fluorescence intensity of major tissues at 4 h pi of Cy5.5-NGR2 (1.5 nmol) with (blocking) and without (non-blocking) co-injection of NGR peptide (20 mg/kg). *Error bar* was calculated as the standard deviation ($n = 3$)

showed significantly higher HT-1080 tumor uptake as compared to that in the blocking group ($P < 0.05$), suggesting the CD13 specificity of Cy5.5-NGR2. Based on the quantitative analysis of ex vivo imaging, the contrast ratios of tumor-to-muscle for the non-blocking and blocking groups were calculated. The tumor-to-muscle ratio at 4 h pi of Cy5.5-NGR2 in the non-blocking and blocking group was determined to be 2.55 ± 0.15 and 0.88 ± 0.09, respectively.

Discussion

In the past decade, significant advances have been made in the field of cancer imaging for both preclinical and clinical research (Weissleder 2006). The achievements largely depend on the development of imaging instrumentation, progresses of cancer molecular and cell biology, and discovery of novel molecular imaging probes (Chen et al. 2004). Various imaging modalities, including PET, SPECT, CT, MR, and optical imaging, have been extensively used to noninvasively evaluate anatomical abnormalities and biofunctional changes in vivo (Atreya et al. 2010; Wagner 2008). For molecular imaging, ^{18}F-fluorodeoxyglucose (^{18}F-FDG) PET has made tremendous success in clinical diagnosis of many cancers. However, ^{18}F-FDG is not a target-specific probe and it cannot differentiate between cells that have a high metabolic rate associated with neoplasia, and those for which the increased metabolic rate is associated with other etiologies, such as infection or inflammation. In addition, many malignancies do not exhibit high metabolic rates and thus, are not properly diagnosed by ^{18}F-FDG (Chen and Chen 2011b). There is a clear demand of developing novel molecular imaging probes to fulfill this urgent and unmet medical need (Weissleder 2006; Shah et al. 2004). Due to the advances in cancer molecular and cell biology, an increasing number of potential molecular targets which are exclusively associated with cancer progression have been revealed. Molecular imaging probes, which can target-specific cancer biomarkers, have a great potential to uncover biological processes in cancer biology, facilitate the individually tailored cancer treatment, and ultimately improve

the outcomes of cancer patients (Chen and Conti 2010). The development of novel molecular imaging probes may focus on not only the nuclear based techniques, but also the non-nuclear based techniques, such as NIRF imaging.

Tumor angiogenesis is a critical process in cancer progression. Without angiogenesis, the tumor may not grow beyond a few millimeters in diameter (Bergers and Benjamin 2003). Increasing evidences have been provided that inhibition of angiogenesis could attenuate tumor growth. A series of angiogenesis inhibitors have shown great potential in cancer treatment (Chen and Chen 2011a). While the progress of the field is encouraging, the clinical benefits of anti-angiogenic agents have been relatively modest thus far, and key questions remain unanswered: in what tumor types, and at what stage(s), should these agents be used? Can novel technologies be developed to identify patients most likely to benefit, or experience toxicities, from treatment? The ultimate impact of anti-angiogenic therapy in the treatment of cancer will likely be determined at least in part by the ability of noninvasive diagnosis techniques, such as molecular imaging, to address these questions (Chen et al. 2012b). Research has shown that CD13 receptor is a critical regulator of angiogenesis. As a cell surface marker, CD13 receptor is overexpressed in many tumor cells (Teranishi et al. 2008; Ikeda et al. 2003; Hashida et al. 2002). NGR-containing peptide has been identified as a specific ligand binding to CD13 receptor (Pasqualini et al. 2000). Therefore, the development of NGR-containing derivatives for targeting CD13 in living subjects is of particular interest, which would allow the noninvasive detection of CD13 expression level and accurate assessment of CD13-targeted treatment efficacy.

In our previous study, we developed a novel dimeric NGR peptide (NGR2), which exhibits excellent binding affinity to CD13 receptor (Chen et al. 2013). A ^{64}Cu-labeled NGR2 probe was subsequently prepared and the resulting ^{64}Cu-NGR2 demonstrated favorable in vivo performance for PET imaging. The motivation of developing non-nuclear-based probe using NGR2 peptide leads us to the design of a fluorophore containing NGR2 peptide. We selected Cy5.5 dye, a widely used and commercially available NIR fluorescent probe, as the fluorescent moiety. To conjugate the Cy5.5 dye with NGR2 peptide, we employed click chemistry approach instead of using conventional amide coupling method. Click chemistry offers chemists a platform for modular and high-yielding synthetic transformations for constructing highly diverse molecules (Kolb and Sharpless 2003). The Huisgen 1,3-dipolar cycloaddition reaction, which fuses an azide and an alkyne together, and provides access to a variety of five-membered heterocycles, has become of great use in the development of new molecular probes (Nwe and Brechbiel 2009). Based on our previous experience (Chen et al. 2012a), we chose a catalyst-free click chemistry system using the ligation of dibenzocyclooctyne and azide (Debets et al. 2010, 2011). To this end, the dimeric NGR peptide (NGR2) was conjugated with an alkyne-containing PEG unit followed by mixing with an azide-terminated Cy5.5 fluorophore (Cy5.5-N_3) to afford Cy5.5-NGR2. The bio-orthogonal click chemistry provided a rapid conjugation of the alkyne-containing NGR2 with Cy5.5-N_3 in a quantitative yield within 15 min. The newly constructed Cy5.5-NGR2 exhibited good NIR property with the maximum absorption and emission wavelength at 674 and 704 nm, respectively (Fig. 2). Cy5.5-NGR2 was then subjected to in vitro testing. The confocal microscopy results clearly demonstrated the target specificity of Cy5.5-NGR2. Interestingly, except for the cell surface binding, the intracellular localization of Cy5.5-NGR2 in HT-1080 cells was also examined (Fig. 3). One possible explanation is the fluorescence dye motif increases lipophilicity of the probe and thus facilitates ligand internalization. Nevertheless, the mechanism of cellular internalization of Cy5.5-NGR2 requires further investigation.

To examine its tumor targeting efficacy, Cy5.5-NGR2 was evaluated in the subcutaneous HT-1080 fibrosarcoma mouse xenografts. In vivo optical imaging studies (Fig. 4) showed that Cy5.5-NGR2 peptide exhibited a fast HT-1080 tumor targeting (as early as 0.5 h pi) and excellent tumor-to-background contrast at 2 h pi in the non-blocking group (Fig. 4). The Cy5.5-NGR2 peptide also displayed good tumor retention. The probe washout in tumor was much slower than normal tissue except for liver and kidneys, leading to good tumor-to-normal tissue contrast at 1–4 h pi. A blocking experiment was achieved by co-injection of Cy5.5-NGR-dimer with unlabeled NGR peptide (20 mg/kg). Significantly reduced tumor uptake ($P < 0.05$) of Cy5.5-NGR2 was observed for the blocking group vs. the non-blocking group at 2 h pi (Fig. 5), indicating Cy5.5-NGR2 peptide is a target-specific probe. Aside from the HT-1080 tumor, liver uptake of Cy5.5-NGR2 peptide remained higher than the amounts measured in other normal organs, suggesting the hepatic pathway as the likely route of Cy5.5-NGR2 excretion (Fig. 6). Further methods to optimize the NIRF NGR2 probe include careful selection of fluorescent labels and improvement of pharmacokinetic profile. We and others have showed that NIR fluorescent dye Cy5.5 can be used as a promising contrast agent for in vivo demarcation of tumors (Weissleder et al. 1999; Tung 2004; Chen et al. 2004, 2012b; Kobayashi et al. 2010). However, the emission maximum of Cy5.5 at 694 nm is at the lower limit of NIRF region. Fluorescent dyes with more red-absorbing character may provide deeper tissue penetration and a better reflection of actual distribution of the probe in vivo. Further modification is also needed to improve pharmacokinetics (PK) of the probe. For

example, an appropriate linker with suitable length, flexibility, hydrophilicity, and charges can be carefully chosen to further tune the PK (Chen and Chen 2010). Our future research plan also includes the development of CD13-targeted theranostics (Xing et al. 2014), which can combine the diagnostic and therapeutic properties in one agent. Based on the results demonstrated in this report, we envision that chemically modified NGR peptide, fluorophores, and chemodrugs can be readily loaded onto functional nanoparticles through bioorthogonal click chemistry. The resulting theranostics may open up new opportunities for CD13-targeted tumor imaging and therapy.

Conclusion

The Cy5.5 fluorophore was successfully conjugated with a dimeric NGR peptide through bioorthogonal click chemistry to afford a Cy5.5-labeled dimeric NGR peptide (Cy5.5-NGR2). The Cy5.5-NGR2 peptide provided highly sensitive and target-specific imaging of CD13 receptor expression in tumors. The excellent tumor-to-normal tissue ratio and fast tumor targeting ability of Cy5.5-NGR2 have proved it a promising molecular probe, not only allowing the NIR optical imaging of CD13-overexpressed tumors, but also having the potential to facilitate non-invasive monitoring of CD13-targeted tumor therapy.

Acknowledgments This work was supported by the USC Department of Radiology, the Major Program of National Natural Science Foundation of China (Grant No. 81230033), the National Basic Research and Development Program of China (Grant No. 2011CB707704), and the Major Research Instrumentation Program of National Natural Science Foundation of China (Grant No. 81227901).

Conflict of interest The authors declare that they have no conflict of interest.

References

Arap W, Pasqualini R, Ruoslahti E (1998) Cancer treatment by targeted drug delivery to tumor vasculature in a mouse model. Science (New York, NY) 279(5349):377–380

Atreya R, Waldner MJ, Neurath MF (2010) Molecular imaging: interaction between basic and clinical science. Gastroenterol Clin North Am 39(4):911–922

Bergers G, Benjamin LE (2003) Tumorigenesis and the angiogenic switch. Nat Rev Cancer 3(6):401–410

Bhagwat SV, Lahdenranta J, Giordano R, Arap W, Pasqualini R, Shapiro LH (2001) CD13/APN is activated by angiogenic signals and is essential for capillary tube formation. Blood 97(3):652–659

Carmeliet P (2000) Mechanisms of angiogenesis and arteriogenesis. Nat Med 6(4):389–395

Chen K, Chen X (2010) Design and development of molecular imaging probes. Curr Top Med Chem 10(12):1227–1236

Chen K, Chen X (2011a) Integrin targeted delivery of chemotherapeutics. Theranostics 1:189–200

Chen K, Chen X (2011b) Positron emission tomography imaging of cancer biology: current status and future prospects. Semin Oncol 38(1):70–86

Chen K, Conti PS (2010) Target-specific delivery of peptide-based probes for PET imaging. Adv Drug Deliv Rev 62(11):1005–1022

Chen X, Conti PS, Moats RA (2004) In vivo near-infrared fluorescence imaging of integrin alphavbeta3 in brain tumor xenografts. Cancer Res 64(21):8009–8014

Chen K, Wang X, Lin W, Shen K-F, Yap LP, Hughes LD, Conti PS (2012a) Strain-promoted catalyst-free click chemistry for rapid construction of ^{64}Cu-labeled PET imaging probes. ACS Med Chem Lett 3(12):1019–1023

Chen K, Yap LP, Park R, Hui X, Wu K, Fan D, Chen X, Conti PS (2012b) A Cy5.5-labeled phage-displayed peptide probe for near-infrared fluorescence imaging of tumor vasculature in living mice. Amino Acids 42(4):1329–1337

Chen K, Ma W, Li G, Wang J, Yang W, Yap LP, Hughes LD, Park R, Conti PS (2013) Synthesis and evaluation of ^{64}Cu-labeled monomeric and dimeric NGR peptides for MicroPET imaging of CD13 receptor expression. Mol Pharm 10(1):417–427

Debets MF, van Berkel SS, Schoffelen S, Rutjes FP, van Hest JC, van Delft FL (2010) Aza-dibenzocyclooctynes for fast and efficient enzyme PEGylation via copper-free (3 + 2) cycloaddition. Chem Commun (Camb) 46(1):97–99

Debets MF, van Berkel SS, Dommerholt J, Dirks AT, Rutjes FP, van Delft FL (2011) Bioconjugation with strained alkenes and alkynes. Acc Chem Res 44(9):805–815

Ellis LM, Liu W, Ahmad SA, Fan F, Jung YD, Shaheen RM, Reinmuth N (2001) Overview of angiogenesis: biologic implications for antiangiogenic therapy. Semin Oncol 28(5 Suppl 16):94–104

Guzman-Rojas L, Rangel R, Salameh A, Edwards JK, Dondossola E, Kim YG, Saghatelian A, Giordano RJ, Kolonin MG, Staquicini FI, Koivunen E, Sidman RL, Arap W, Pasqualini R (2012) Cooperative effects of aminopeptidase N (CD13) expressed by nonmalignant and cancer cells within the tumor microenvironment. Proc Natl Acad Sci USA 109(5):1637–1642

Hashida H, Takabayashi A, Kanai M, Adachi M, Kondo K, Kohno N, Yamaoka Y, Miyake M (2002) Aminopeptidase N is involved in cell motility and angiogenesis: its clinical significance in human colon cancer. Gastroenterology 122(2):376–386

Ikeda N, Nakajima Y, Tokuhara T, Hattori N, Sho M, Kanehiro H, Miyake M (2003) Clinical significance of aminopeptidase N/CD13 expression in human pancreatic carcinoma. Clin Cancer Res Off J Am Assoc Cancer Res 9(4):1503–1508

Kobayashi H, Ogawa M, Alford R, Choyke PL, Urano Y (2010) New strategies for fluorescent probe design in medical diagnostic imaging. Chem Rev 110(5):2620–2640

Kolb HC, Sharpless KB (2003) The growing impact of click chemistry on drug discovery. Drug Discov Today 8(24): 1128–1137

Kuwano M, Fukushi J, Okamoto M, Nishie A, Goto H, Ishibashi T, Ono M (2001) Angiogenesis factors. Intern Med 40(7):565–572

Luan Y, Xu W (2007) The structure and main functions of aminopeptidase N. Curr Med Chem 14(6):639–647

Negussie AH, Miller JL, Reddy G, Drake SK, Wood BJ, Dreher MR (2010) Synthesis and in vitro evaluation of cyclic NGR peptide targeted thermally sensitive liposome. J Control Release Off J Control Release Soc 143(2):265–273

Nwe K, Brechbiel MW (2009) Growing applications of "click chemistry" for bioconjugation in contemporary biomedical research. Cancer Biother Radiopharm 24(3):289–302

Pasqualini R, Koivunen E, Kain R, Lahdenranta J, Sakamoto M, Stryhn A, Ashmun RA, Shapiro LH, Arap W, Ruoslahti E (2000)

Aminopeptidase N is a receptor for tumor-homing peptides and a target for inhibiting angiogenesis. Cancer Res 60(3):722–727

Raymond SB, Skoch J, Hills ID, Nesterov EE, Swager TM, Bacskai BJ (2008) Smart optical probes for near-infrared fluorescence imaging of Alzheimer's disease pathology. Eur J Nucl Med Mol Imaging 35(Suppl 1):S93–S98

Sakatani K, Kashiwasake-Jibu M, Taka Y, Wang S, Zuo H, Yamamoto K, Shimizu K (1997) Noninvasive optical imaging of the subarachnoid space and cerebrospinal fluid pathways based on near-infrared fluorescence. J Neurosurg 87(5):738–745

Shah K, Jacobs A, Breakefield XO, Weissleder R (2004) Molecular imaging of gene therapy for cancer. Gene Ther 11(15):1175–1187

Teranishi J, Ishiguro H, Hoshino K, Noguchi K, Kubota Y, Uemura H (2008) Evaluation of role of angiotensin III and aminopeptidases in prostate cancer cells. Prostate 68(15):1666–1673

Tung CH (2004) Fluorescent peptide probes for in vivo diagnostic imaging. Biopolymers 76(5):391–403

von Wallbrunn A, Waldeck J, Holtke C, Zuhlsdorf M, Mesters R, Heindel W, Schafers M, Bremer C (2008) In vivo optical imaging of CD13/APN-expression in tumor xenografts. J Biomed Optics 13(1):011007

Wagner HN Jr (2008) Advancing a molecular theory of disease. J Nucl Med 49(8):15N–34N

Wang RE, Niu Y, Wu H, Amin MN, Cai J (2011) Development of NGR peptide-based agents for tumor imaging. Am J Nucl Med Mol Imaging 1(1):36–46

Weissleder R (2006) Molecular imaging in cancer. Science 312(5777):1168–1171

Weissleder R, Tung CH, Mahmood U, Bogdanov A Jr (1999) In vivo imaging of tumors with protease-activated near-infrared fluorescent probes. Nat Biotechnol 17(4):375–378

Wunderbaldinger P, Turetschek K, Bremer C (2003) Near-infrared fluorescence imaging of lymph nodes using a new enzyme sensing activatable macromolecular optical probe. Eur Radiol 13(9):2206–2211

Xing Y, Zhao J, Conti PS, Chen K (2014) Radiolabeled nanoparticles for multimodality tumor imaging. Theranostics 4(3):290–306

Yancopoulos GD, Davis S, Gale NW, Rudge JS, Wiegand SJ, Holash J (2000) Vascular-specific growth factors and blood vessel formation. Nature 407(6801):242–248